Raman scattering and infrared reflectivity in $[(InP)_5(In_{0.49}Ga_{0.51}As)_8]_{30}$ superlattices

Z. V. Popović,[a] A. Cantarero,[b] and J. Camacho
Materials Science Institute, University of Valencia, 46100 Burjasot (Valencia), Spain

A. Milutinovi and O. Latinovi
Institute of Physics, 11080 Belgrade, P.O. Box 68, Yugoslavia

L. González
Instituto de Microelectrónica de Madrid, CNM-CSIC, PTM, 28760 Tres Cantos (Madrid), Spain

We have measured far-infrared and infrared reflectivity as well as Raman scattering in an $[(InP)_5(In_{0.49}Ga_{0.51}As)_8]_{30}$ superlattice grown by molecular beam epitaxy. A numerical model for calculating the reflectivity coefficient for complex systems which includes superlattice, buffer layer, and substrate has been developed. The far-infrared reflectivity spectra consists of the superlattice confined and interface modes as well as the modes from the buffer layer $(In_{0.49}Ga_{0.51}As)$ and the substrate (InP). In the infrared spectral range above 1000 cm^{-1} we observe only interference fringes from the buffer layer. A good agreement between calculated and experimental spectra is achieved. The folded longitudinal acoustic phonon doublet appears at about 39 cm^{-1} in the Raman scattering spectra. The frequency agrees well with a continuum model calculation. In the optical phonon spectral region we observe confined modes corresponding to both constituents. The modes representing vibrations of atoms at both interfaces: InP/InGaAs (230 cm^{-1} mode) and InGaAs/InP (240 and 260 cm^{-1} modes) have also been observed. The geometrical parameters of the sample, obtained from the fitting of the reflectivity data, agree well to the values of the layer thickness obtained by double crystal x-ray diffraction. © *2000 American Institute of Physics.* [S0021-8979(00)01017-3]

I. INTRODUCTION

In$_x$Ga$_{1-x}$As/InP is a very attractive material system of considerable interest for applications in modern optoelectronic devices and high-speed electronics.[1] In spite of the great interest in this kind of systems, there are only a few works related to the characterization of the confined phonons and interface modes in the InP/InGaP heterojunction. It is well known that the performance of real devices is enhanced by the quality of the interfaces. In the case of In$_x$Ga$_{1-x}$As/InP superlattices (SPs) it has been suggested that undesired strain layers, a few monolayers thick, are present at both InP–InGaAs and InGaAs–InP interfaces. Recently, Boscherini *et al.*[2] have demonstrated the presence of unwanted interface layers between InP and In$_x$Ga$_{1-x}$As (and vice versa) using x-ray atomic force spectroscopy (XAFS). They modeled the structure as composed by the two nominal layers plus In$_x$As$_{1-x}$P and In$_{0.53}$Ga$_{0.47}$As$_{1-y}$P$_y$ strained interface layers. The presence of these interface layers has also become necessary to interpret magnetophotoluminescence measurements of InGaAs/InP multiquantum barriers.[3] The characterization of the interface abruptness of lattice-matched InGaAs/InP multiquantum wells by Raman spectroscopy is given in Refs. 4 and 5. On one hand, the interface-like peaks around 240 and 260 cm^{-1} are shown to

be related to the InGaAs/InP interface. Geurts *et al.*[5] have assigned these peaks to In–As and Ga–As vibrational modes of quarternary InGaAsP layers, which originate from the exchange between P and As atoms at the InGaAs surface during purging prior to the InP molecular organic chemical vapor deposition (MOCVD) growth. On the other hand, the peak which appears at about 230 cm^{-1} is assigned to the In–As vibration of InAsP, formed due to a carry-over of the As precursor into the next InP layer.[4]

In this article we have used far-infrared and infrared spectroscopy as well as Raman scattering measurements to characterize an InP/InGaAs superlattice grown by molecular beam epitaxy (MBE) techniques. For the analysis of the infrared reflectivity (IR) spectra we have developed a model which includes superlattice, interface, buffer, and substrate layer properties in the calculation of the coefficient of reflection. A good agreement between measured and calculated spectra is achieved. The Raman spectra shows folded phonon doublet as well as confined and interface phonon modes. The geometrical parameters obtained by the fitting procedure of infrared and far-infrared reflectivity spectra are in accordance with the x-ray diffraction data.

II. EXPERIMENTAL DETAILS

A practically unstrained $[(InP)_5(In_{0.49}Ga_{0.51}As)_8]_{30}$ superlattice with a buffer layer of In$_{0.49}$Ga$_{0.51}$As was grown on a (001)-oriented InP substrate using molecular beam epitaxy. The sample was grown by solid source atomic layer molecu-

[a]On leave from Institute of Physics, 11080 Belgrade, P.O. Box 68, Yugoslavia.
[b]Electronic address: cantarer@uv.es; URL: http://www.uv.es/~cantarer

lar beam epitaxy (ALMBE) at a substrate temperature T_s $=425\,°C$. The actual period of superlattice was measured with a high-resolution double-crystal x-ray diffractometer. The thickness of the individual InP and InGaAs layers were determined to be 14 and 23 Å , respectively. The thickness of the monolayers in the (001) direction is $a_0/2$, where a_0 represents the bulk lattice constants, 5.8687 and 5.8518 Å for (InP) and ($In_{0.49}Ga_{0.51}As$), respectively; thus the number of monolayers in the superlattice studied is 5 and 8 of InP and InGaAs, respectively. The lattice mismatch is only 0.3% at room temperature. The thickness of the buffer layer is 5005 Å and significantly exceeds the critical thickness $t_c = 200$ Å[6] in such a way that misfit dislocations which were produced during the growth, accommodate the strain energy and permit the buffer layer to relax to its natural, bulk, lattice constant.

The infrared measurements were carried out with a BOMEM DA-8 FIR spectrometer. A DTGS pyroelectric detector was used to cover the wave number range from 100 to 700 cm^{-1}; a liquid nitrogen cooled HgCdTe detector was used from 500 to 5000 cm^{-1}. The spectra were collected with 1 cm^{-1} resolution. The Raman spectra were measured in backscattering configuration using micro-(macro)–Raman systems with a Dilor (Jobin Yvon) triple (double) monochromator including liquid nitrogen (Peltier effect) cooled charge-coupled device (CCD)-(photomultiplier) detector. An Ar ion laser was used as excitation source.

III. THE PROPAGATION OF ELECTROMAGNETIC WAVES THROUGH SUPERLATTICES

The penetration depth of the infrared electromagnetic waves into a nontransparent crystal is about 3 μm. The superlattice thickness is usually less than 1 μm, as the investigated one, and the reflectivity spectra, in general, contains information from the superlattice together with information from the substrate and additional layers (buffer) if the investigated sample contains them.

We shall briefly review the propagation of plane monochromatic electromagnetic waves with near normal incidence in absorbing uniaxial crystal films on isotropic substrates. Figure 1 schematically presents a three-layer structure with corresponding dielectric constants ϵ_1, ϵ_2, and ϵ_3. If medium "1" is air with dielectric constant ϵ_1 ($=1$), medium "2" is a thin absorbing crystal layer (superlattice) with $\epsilon_2 = \epsilon_{SL}$, and medium "3" is a substrate with $\epsilon_3 = \epsilon_S$, then the amplitude of the reflected beam becomes[7,8]

$$A_r = A_i[\mathbf{r}_{12} + (\mathbf{t}_{12}\mathbf{t}_{21})\mathbf{r}_{23} e^{2i\alpha} + (\mathbf{t}_{12}\mathbf{t}_{21})\mathbf{r}_{21}\mathbf{r}_{23}^2 e^{4i\alpha}$$
$$+ (\mathbf{t}_{12}\mathbf{t}_{21})\mathbf{r}_{21}^2\mathbf{r}_{23}^3 e^{6i\alpha} + \cdots], \tag{1}$$

where A_i is the amplitude of the incident beam; $\alpha = 2\pi\omega d\sqrt{\epsilon_{SL}}$ the complex phase change related to the absorption in the crystal layer with thickness $d = d_{SL}$; $\mathbf{r}_{12}$, $\mathbf{r}_{21}$, $\mathbf{r}_{23}$, $\mathbf{t}_{12}$, and $\mathbf{t}_{21}$ are the Fresnel coefficients of reflection and transmission on the "1–2," "2–1," and "2–3" interfaces, respectively, expressed by complex refractive indices n, or dielectric constants ϵ:
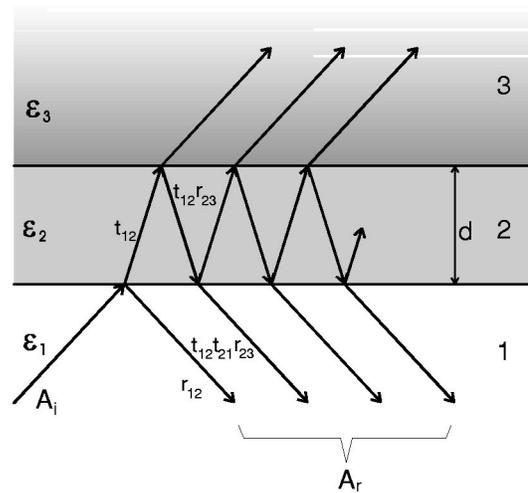
FIG. 1. A schematic presentation of a three-layer structure with corresponding dielectric constants ϵ_1, ϵ_2, and ϵ_3.

$$\mathbf{r}_{21} = -\mathbf{r}_{12} = \frac{n_2 - n_1}{n_2 + n_1} = \frac{\sqrt{\epsilon_2} - \sqrt{\epsilon_1}}{\sqrt{\epsilon_2} + \sqrt{\epsilon_1}} \quad ,$$

$$\mathbf{r}_{23} = \frac{n_2 - n_3}{n_2 + n_3} = \frac{\sqrt{\epsilon_2} - \sqrt{\epsilon_3}}{\sqrt{\epsilon_2} + \sqrt{\epsilon_3}} \quad , \tag{2}$$

$$\mathbf{t}_{12}\mathbf{t}_{21} = 1 - \mathbf{r}_{12}^2 = \frac{4n_1 n_2}{n_1 + n_2} = \frac{4\sqrt{\epsilon_1 \epsilon_2}}{\sqrt{\epsilon_1} + \sqrt{\epsilon_2}} \quad .$$

Summing the components given by a series that takes into account multiple-beam interference effects [Eq.(1)], results in the following expression:

$$R_A = \frac{A_r}{A_i} = \frac{\mathbf{r}_{12} e^{-i\alpha} + \mathbf{r}_{23} e^{i\alpha}}{e^{-i\alpha} + \mathbf{r}_{12}\mathbf{r}_{23} e^{i\alpha}} \quad . \tag{3}$$

The reflectance of the crystal thin film (superlattice) on the isotropic semi-infinite substrate, after introducing Eq. (2) into Eq. (3), becomes

$$\mathbf{R} = \left| \frac{[1 - 1/\sqrt{\epsilon_S}]\cos\alpha - i[\sqrt{\epsilon_{SL}/\epsilon_S} - 1/\sqrt{\epsilon_{SL}}]\sin\alpha}{[1 + 1/\sqrt{\epsilon_S}]\cos\alpha - i[\sqrt{\epsilon_{SL}/\epsilon_S} + 1/\sqrt{\epsilon_{SL}}]\sin\alpha} \right|^2 . \tag{4}$$

The dielectric constants of the superlattice constituents and the substrate, which takes into account the absorption of the lattice vibrations, are given in factorized form as

$$\epsilon = \epsilon_\infty \prod_{j=1}^{n} \frac{\omega_{LOj}^2 - \omega^2 + i\gamma_{LOj}\omega}{\omega_{TOj}^2 - \omega^2 + i\gamma_{TOj}\omega} \quad , \tag{5}$$

where ω_{TO} and ω_{LO} are the transverse and longitudinal optical vibrations, γ_{TO} and γ_{LO} their damping constants, and ϵ_∞ the high-frequency dielectric constant. The superlattice is treated as a unique uniaxial crystal layer with a dielectric constant which corresponds to the effective medium model[6]

$$\epsilon_{SL} = \epsilon_{eff} = \frac{\Sigma_i d_i \epsilon_i}{\Sigma_i d_i} \quad , \tag{6}$$

where ϵ_i (d_i) denotes the dielectric constant (thickness) of the SL constituents. Equation (4) was successfully applied in the calculation of the reflection coefficient of superlattices on isotropic substrates[9–11] without buffer layers.

If an additional crystal layer exists between the superlattice and the substrate (a buffer layer, for example, with a lattice parameter different from the substrate), the multibeam reflectance analysis becomes more complex. Zeng *et al.*[12] have suggested a rather simple way for solving the problem of the reflection on multilayer structures by iteration including the effects of single layers. Using this idea, the $\mathbf{r}_{23}$ coefficient, in the case of one additional layer between substrate and superlattice, becomes

$$\mathbf{r}_{23} = \frac{\mathbf{r}_{23}\, e^{-i\beta} + \mathbf{r}_{34}\, e^{i\beta}}{e^{-i\beta} + \mathbf{r}_{23}\mathbf{r}_{34}\, e^{i\beta}} \quad , \tag{7}$$

$\beta = 2\pi\omega d_B \sqrt{\epsilon_B}$ being the complex phase change due to the absorption in the buffer layer of thickness d_B. The reflection coefficient $\mathbf{r}_{34}$ now becomes

$$\mathbf{r}_{34} = \frac{n_3 - n_4}{n_3 + n_4} \quad , \tag{8}$$

where n_3 the refractive index of the buffer layer and n_4 the one of the substrate. In the same way it is possible to include additional layers in the calculations of the reflection coefficient.

IV. RESULTS AND DISCUSSION

There are three types of phonons in superlattices. The confined optical phonons are the result of the inability of two SL constituents to vibrate with the same optic frequencies due to different atomic masses and/or different force constants. The energy gap between the optical dispersion branches of the constituents causes the damping of one constituent vibrations by the adjacent layers of the other constituent. This confinement leads to the formation of standing waves in the growth direction with nodes near the interfaces. Each mode confined in a layer with thickness d_i has an effective wave vector which depends on the order m of the confined mode and the effective layer thickness d_i

$$q_m = \frac{m\pi}{d_i}, \quad m = \pm 1, \pm 2, \pm 3, \dots . \tag{9}$$

A superlattice exhibits a new periodicity $d = d_1 + d_2$ along the growth direction and its unit cell becomes larger than the unit cell of the SL constituents. In consequence, mini Brillouin zones (MBZ) are formed, by folding the dispersion curves of the bulk material. This folding produces modes with SL wave vector $q_{SL} = 0$, but with frequencies different from zero, so these modes are observable in Raman scattering spectra.

The interface modes originated from the dielectric constant difference (discontinuity) at the interfaces of the SL constituents. These Raman inactive modes, with wave vectors in the SL layers plane, appear in the Raman spectra owing to a deviation from the strict backscattering geometry or to interface imperfections. The interface modes are between LO and TO confined modes frequencies.
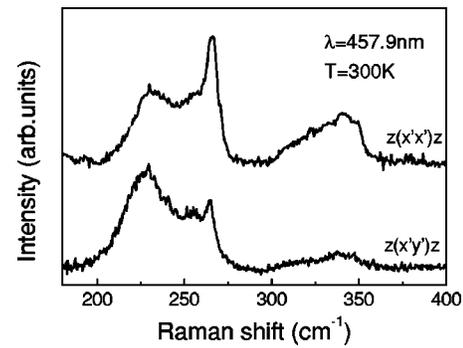
FIG. 2. Raman spectra of the $[(\text{InP})_5(\text{In}_{0.49}\text{Ga}_{0.51}\text{As})_8]_{30}$ superlattice measured at room temperature with parallel and crossed polarization.

The properties of all mentioned phonons in superlattices have been previously discussed.[13] In the case of (001) oriented superlattice with ZnS-type crystal structure constituents it is possible to observe longitudinal optic (LO$_m$) confined modes as well as longitudinal acoustic (LA) folded phonon modes in the backscattering geometry. For parallel polarization $(x'x')$, $(y'y')$, where $x' = [110]$, $y' = [1\bar{1}0]$, both $m = (\text{odd, even})$ LO$_m$ confined modes are expected in Raman spectra. For crossed polarizations $(x'y')$ the Raman modes are forbidden.[14]

The Raman spectra of our SL sample in the optical phonon region for parallel and crossed polarizations are given in Fig. 2. These spectra were measured at room temperature with the 457.9 nm laser line. At this excitation wavelengths the contribution of the buffer layer to Raman scattering is negligible. Namely, the penetration depth is proportional to $1/\alpha = \lambda/4\pi\kappa$, where α is the absorption coefficient and κ is imaginary part of the complex refractive index. Using the values of κ for InP, InAs, and GaAs at 514.5 nm,[15] the penetration depth is around 1100 Å. Consequently, the collected Raman signal originated from the first 1100 Å of the sample and the thickness of our SL sample exceeds a little that limit (there is less absorption at 457.9 nm).

As it can be seen in Fig. 2 there are two sets of SL peaks arising from the In$_{0.49}$Ga$_{0.51}$As and InP optic phonons in the ranges 220–270 cm^{-1} and 300–350 cm^{-1}, respectively. The frequency position of these modes were extracted by a Lorentzian contour deconvolution technique, as it is shown in Fig. 3. The identification of the bands in the In$_{0.49}$Ga$_{0.51}$As range was done in terms of a two-mode behavior for optical phonons of the bulk material.[16–19] LO phonons can be considered to be confined to the individual layers due to the large energy separation between the optical bands of InP and In$_{0.49}$Ga$_{0.51}$As. To our knowledge, neither neutron scattering data nor dispersion relations exist for the In$_{1-x}$Ga$_x$As system, except the theoretical dispersion calculated for InGaAs$_2$.[20] The theoretical curves for GaAs-like and InAs-like vibrations are lower than one could expect. The LO-dispersion curves for InGaAs$_2$, which correspond to GaAs-like oscillations are almost dispersionless. Thus, confined modes could not be resolved. On the other hand, the InAs-like LO frequency increases with the wave vector and the corresponding confined modes frequencies are expected to be higher than the frequency of the bulk material. It is obvi-
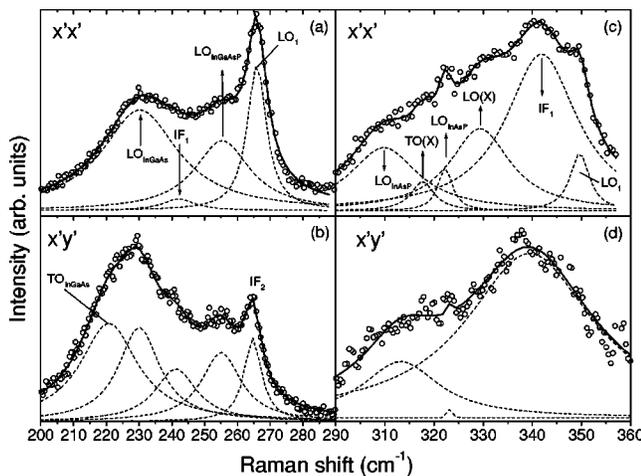
FIG. 3. Raman spectra of the $[(InP)_5(In_{0.49}Ga_{0.51}As)_8]_{30}$ superlattice in the optical phonon region of InP and InGaAs deconvoluted by Lorentzian line profiles.

FIG. 4. Phonon dispersion curves of InP calculated using a bond-charge model. Experimental data for $\mathbf{q}=0$ (Raman) and $\mathbf{q}>0$ (neutron) are shown by open (LO) and solid (TO) circles, respectively (see Ref. 23).

ous that only the mode at 266 cm^{-1} has LO character. This mode can be assigned as LO$_1$ mode. For $(x'x')$ polarization we can expect the appearance of LO$_m$ modes with m odd and even. Because the GaAs like optical branch is practically dispersionless,[20] this mode can be the superposition of several LO$_m$ modes. For crossed polarizations $(x'y')$, Fig. 3(b), this mode weakens and shifts to lower energies. Because of that, we assigned this mode to an interface ($\mathbf{q}$ in plane) mode. The other three optical modes from Fig. 3(a) at about 230, 242, and 255 cm^{-1} also appear in crossed polarizations [Fig. 3(b)]. This means that these modes are not confined modes. We assign these modes to an InGaAs alloy mode, an interface mode, and an InGaAsP alloy mode, respectively. The support for this assignment can be found in Refs. 18 and 21. Namely, Quagliano *et al.*[21] have investigated the vibrational properties of thin InAs layer directly grown on InP substrate. They resolved broad bands at about 232 and 322 cm^{-1} originated from atomic vibrations of the ternary alloy InAsP. This alloy is formed by the incorporation of arsenic on the InP substrate (in our case on the next InP layer). The mode around 230 cm^{-1} is also found in Refs. 4 and 5. Besides the broad structures, Quagliano *et al.* have found intense narrow lines at about 244, 343, and 311 cm^{-1}, which they assigned as InAs, InP, and InAsP interface modes. Besides that, Guerts *et al.*,[5] showed that the two modes at 240 and 260 cm^{-1} can be assigned to the quaternary InGaAsP alloy mode, which appears at the InGaAs/InP interfaces. The lowest frequency mode in Fig. 3(b) at about 221 cm^{-1} is a TO like InGaAs IF mode.

In the InP optical phonon region [Figs. 3(c) and (d)] we have resolved the LO$_1$ confined mode of InP at about 349 cm^{-1}, the InP interface mode at 342 cm^{-1}, the InAsP alloy mode at 322 cm^{-1}, and TO-like InAsP interface mode at about 311 cm^{-1}. Besides these modes, two additional broad modes at about 318 and 329 cm^{-1} are observed. We assign these modes as TO(X) and LO(X) modes, respectively. According to neutron scattering data shown in Fig. 4,[22] there are several modes around these frequencies. This produces a high density of phonon states near the X point of the Bril-

louin zone edge. Thus, these modes can also be observed in Raman scattering. The appearance of all mentioned "Raman forbidden" (interface-like) modes in the spectra for parallel polarization is a consequence of the relaxation of selection rules induced by interface disorder.
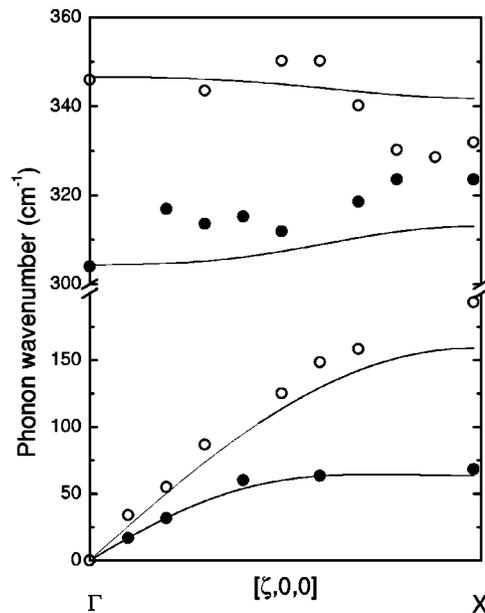
The continuous line in Fig. 4 shows the dispersion relation calculations for InP calculated by means of a bond-charge model. The model parameters were taken from the literature.[23] There is no satisfactory agreement between the neutron scattering data and the calculated curves, as already stated by a bond-bending force model.[24] We also found that neutron and Raman scattering data differ significantly. We believe that new neutron data are necessary to clarify this problem.

Raman scattering by folded acoustic phonons in (001) and high-index plane (hkl) GaAs/AlAs superlattices is well documented.[13,25] As predicted by selection rules for (001)-oriented superlattices of zinc-blende crystal structure, only the LA component is Raman active. Figure 5 shows the Raman spectra for (xx) polarization in the spectral range 30 and 50 cm^{-1} obtained at 300 K with 514.5 nm line of an Ar$^+$ ion laser. The doublet $(-1,+1)$ of the folded LA-phonon modes at 37.5 and 42 cm^{-1} is clearly observed. We have compared the frequencies of the observed folded-phonon modes with a calculation based on a continuum model. Folded-phonon dispersion curves calculated with this model are given in the inset of Fig. 5 together with the experimental frequencies obtained with the 514.5 nm line of an Ar$^+$ ion laser. Our experimental data for the LA folded phonons in the InP/InGaAs superlattice are fully in agreement with the continuum model calculation, which means that the stiffness constants, taken from the bulk materials[26,27] are correct. Sharp and well defined folded phonons are evidence of abrupt interfaces in the sample.
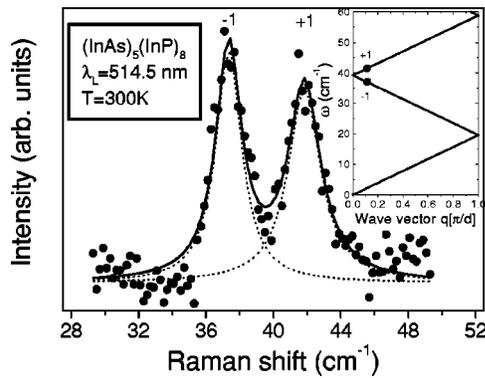
FIG. 5. Raman spectra of the $[(InP)_5(In_{0.49}Ga_{0.51}As)_8]_{30}$ superlattice in the spectral range from 30 to 50 cm^{-1} measured with the 514.5 nm line of an Ar$^+$ ion laser at 300 K. The inset shows the continuum-model results for folded-phonon dispersion curves together with experimentally observed LA folded phonons.

TABLE I. Optical parameters used in the present study (frequencies and damping coefficients are in cm^{-1}).

ω_{TOj}	γ_{TOj}	ω_{LOj}	γ_{LOj}	ϵ_∞	
302	2	345	2	9.6	InP-substrate
228.8	12	234	16	12.3	Buffer-InAs
255	10	275	11	10.8	Buffer-GaAs
231	7	233	9		InAsP alloy
241	6	243	3		IF InAsP
245	6	257	9		InGaAsP alloy
252	8	265	7		InGaAsP alloy
303	5	345	1.5		LO$_1$ InP

The far-infrared and infrared reflectivity spectra of the $[(InP)_5(In_{0.49}Ga_{0.51}As)_8]_{30}$ superlattice is presented in Fig. 6. Circles are experimental data and the solid line is the calculated spectra obtained by the fitting procedure described in Sec. III. The best fit parameters are presented in Table I. These parameters, together with the geometrical parameters $d_{InP}=14$ Å and $d_{In_{0.49}Ga_{0.51}As}=23$ Å, $L=30$ Å, and $d_B=5550$ Å, give the best fit between the experimentally obtained spectra and the calculated ones. The highest intensity oscillator in the far-infrared region around 300 cm^{-1} represents a superposition of the lattice vibration of the InP substrate mode and the SL confined mode. The complex structure between 220 and 270 cm^{-1} (inset in Fig. 6) contains oscillators from the superlattice, buffer, and interface layers as further discussed. It is obvious that the values of the SL geometrical parameters obtained from the fitting procedure are in excellent agreement with those obtained with x-ray diffraction techniques.

The confined mode in the superlattice could not be completely resolved in the Fourier infrared (FIR) spectra given in Fig. 6. The InP confined modes are hidden by the strong substrate peak, but it was necessary to include at least one confined InP mode in the fitting procedure in order to obtain good agreement with the experimental data.

Two more well pronounced modes in the inset of Fig. 6 are the bulk modes of the $In_{0.49}Ga_{0.51}As$ buffer layer; the other modes observed are the confined modes of the $In_{0.49}Ga_{0.51}As$ component of the superlattice or interface modes. The TO and LO frequencies of the buffer layer are the same as for the bulk. The intensity of the modes in the buffer observed in the FIR spectra is stronger than that of the SL confined modes because the thickness of the buffer layer is larger. The complete assignment of all observed modes in far-infrared spectra is given in Table I and we do not repeat it here again. We have also found a very good agreement between infrared and Raman mode frequencies.

V. CONCLUSIONS

Far infrared and Raman scattering have been used to characterize the InP/InGaP interface. This gives us a complete picture of all the optical modes, confined and interface modes, as well as folded acoustic phonon modes in the heterojunction. For the analysis of the IR reflectivity spectra we have developed a model which includes superlattice, interface, buffer, and substrate layer properties in calculating the reflection coefficient. A good agreement between measured and calculated spectra is achieved using the geometrical parameters obtained from the fitting procedure of infrared and far-infrared reflectivity spectra agree well with the x-ray diffraction data. The Raman spectra shows folded phonon doublet as well as confined and interface phonon modes.

FIG. 6. Infrared reflectivity of the $[(InP_5(In_{0.49}Ga_{0.51}As)_8]_{30}$ superlattice measured at 300 K. Open circles are experimental data and the solid line represents the calculated spectra obtained by a fitting procedure. Inset: the same spectra in the 220–270 cm^{-1} spectral region.

[1] A. M. K. *et al.*, IEEE Electron Device Lett. **14**, 36 (1992).
[2] F. Boscherini, C. Lamberti, S. Pascarelli, C. Rigo, and S. Mobilio, Phys. Rev. B **58**, 10745 (1998).
[3] F. Liaci, D. Greco, R. Cingolani, D. Campi, C. Rigo, and D. Soldani, Solid State Commun. **105**, 279 (1998).
[4] J. Geurts, J. Finders, J. Woitok, D. Gnoth, A. Kohl, and K. Heine, J. Cryst. Growth **145**, 813 (1994).
[5] J. Geurts, D. Gnoth, J. Finders, A. Kohl, and K. Heine, Phys. Status Solidi A **152**, 211 (1995).

[6] V. M. Agranovich and V. E. Kravtsov, Solid State Commun. **55**, 85 (1985).

[7] O. Piro, Phys. Rev. B **36**, 3427 (1987).

[8] G. A. Swallow and G. C. Allen, Oxid. Met. **17**, 141 (1982).

[9] B. Lou, Solid State Commun. **76**, 1395 (1990).

[10] G. Scamarcio, L. Tapfer, W. Konig, K. Ploog, and A. Cingolani, Appl. Phys. A: Solids Surf. **51**, 252 (1990).

[11] G. Scamarcio, L. Tapfer, W. Konig, A. Fisher, K. Ploog, E. Molinari, S. Baroni, P. Giannozzi, and S. D. Gironcoli, Phys. Rev. B **43**, 14754 (1991).

[12] A. Zeng, J. Eldridge, C. Lavoie, and T. Tiedje, Solid State Commun. **87**, 1039 (1993).

[13] B. Jusserand and M. Cardona, in *Light Scattering in Solids V*, edited by M. Cardona and G. Güntherodt (Springer, Berlin, 1988), No. 66 in Topics in Applied Physics, Chap. 3, pp. 49–152.

[14] Z. V. Popovi, Univ. Beograd, Publ. Elektrotehn. Fak. Ser. The. Fiz.**1**, 5 (1992).

[15] *Handbook of Optical Constants of Solids*, edited by E. D. Palik (Academic, Orlando, 1985).

[16] J. P. Estrera, P. D. Stevens, R. Glosser, W. M. Duncan, Y. C. Kao, H. Y Liu, and E. A. B. III, Appl. Phys. Lett. **61**, 1927 (1992).

[17] S. Yamazaki, A. Ushirokawa, and T. Katoda, J. Appl. Phys. **51**, 3722 (1980).

[18] T. P. Pearsall, R. Carles, and J. Portal, Appl. Phys. Lett. **42**, 436 (1983).

[19] Z. C. Feng, A. A. Allerman, P. A. Barnes, and S. Perkowitz, Appl. Phys. Lett. **60**, 1848 (1992).

[20] A. Mintairov and H. Temkin, Phys. Rev. B **55**, 5117 (1997).

[21] L. G. Quagliano, B. Jusserand, and D. Orani, in *Proceedings of the 16th International Conference on Raman Spectroscopy*, edited by A. M. Heyns (Wiley, Cape Town, 1998), p. 646.

[22] P. H. Borcherds, G. A. D. G. Saunderson, and A. D. B. Woods, J. Phys. C **8**, 2002 (1975).

[23] S. K. Yip and Y. C. Chang, Phys. Rev. B **30**, 7037 (1984).

[24] M. S. Kushwana and S. Kushwana, Can. J. Phys. **58**, 351 (1980).

[25] S. J. Spitzer, Z. V. Popović, T. Ruf, M. Cardona, R. Nötzel, and K. Ploog, Solid-State Electron. **37**, 753 (1994).

[26] *Semiconductors Basic Data*, edited by O. Madelung (Springer, Berlin, 1966).

[27] R. Merlin, *Properties of Lattice-Matched and Strained InGaAs*, edited by P. Bhattacharya (Inspec, London, 1993), p. 192.